On the Principles of Tweaking Nanostructure Fabrication via Focused Electron Beam Induced Processing Combined with Catalytic Growth Processes

*Martin Drost, Fan Tu, Florian Vollnhals, Imre Szenti, Janos Kiss, and Hubertus Marbach**

Novel pathways to use a focused electron beam in ultrahigh vacuum in combination with catalytic growth protocols are explored for the fabrication of well-defined nanostructures. Thereby, the basic process is the local deposition of material from different precursor molecules ($Co(CO)_3$ NO, $Fe(CO)_5$). This can be realized with a focused electron beam by direct deposition of the precursor or by a chemical modification of the substrate, such that it becomes activated toward the decomposition of the precursor. For both methods, autocatalytic growth (AG) processes can occur, yielding the deposition of additional material. Interestingly, significantly different chemical selectivities for the two precursors are found, which can drastically change upon subtle changes of the surface. It is demonstrated that AG can be tweaked by the choice of the substrate/precursor combination. One possibility to quench catalytic activity of a substrate is the preparation of a thin layer of organic molecules, here porphyrins, which enables the fabrication of hybrid metal–organic nanostructures with line widths below 20 nm. Based on these findings, corresponding techniques are developed which exploit (auto)catalytic effects for the controlled fabrication of nanostructures. These results indicate that every substrate is applicable to electron beam induced surface activation by preparation of a thin porphyrin layer.

1. Introduction

During the past 10 to 15 years, focused electron beam induced processing (FEBIP) has emerged as a powerful lithographic method to fabricate arbitrarily shaped nanostructures on surfaces.[1–3] Current applications include prototype fabrication, e.g., of field emitters[4] and sharp tips for magnetic force microscopy,[5] and photomask repair in semiconductor industry.[6] FEBIP encompasses several mask-less direct write techniques, with electron beam induced deposition (EBID) being the most prominent. In EBID, a suitable precursor compound is adsorbed on a surface and dissociated by the focused beam of an electron microscope. In an ideal EBID process (shown in **Figure 1**(1)), undesired volatile dissociation products desorb, and a deposit remains at the point of impact of the electron beam. The extent of the deposit is usually larger than the beam spot size due to the contribution of backscattered, secondary and forward scattered electrons.[7–12] Consequently, an increase in primary electron (PE) dose leads to more deposited material when the deposition occurs in the electron limited regime.[1] The vast amount of available precursor compounds is a distinct advantage of the technique; however, precise control over the chemical composition of the deposit is a major challenge.

Metal contents ranging from <10 at% (e.g., Pt from $C_5H_5Pt(CH_3)_3$, Mo from $Mo(CO)_6$[13]) up to >90 at% (e.g., Fe from $Fe(CO)_5$,[14] Co from $Co_2(CO)_8$,[15] Au from $(CH_3)_2(C_5H_7O_2)Au$[16]) have been reported (see also ref. [17]), with impurities including precursor and residual gas fragments, the most common ones being carbon and oxygen. In order to fabricate nanostructures with defined properties, identifying, understanding, and ultimately controlling the dissociation and growth processes is an essential goal in FEBIP.

Another recently explored FEBIP technique is electron beam induced surface activation (EBISA).[18,19] In EBISA, the surface is first irradiated with the electron beam in the absence of a precursor (Figure 1(1)). This leads to a chemical modification of the irradiated surface sites such that they become catalytically active toward the decomposition of a subsequently dosed precursor, resulting in the formation of a deposit. EBISA has already been found to work with a variety of precursor/substrate combinations: $Fe(CO)_5$ on SiO_x[12,19–21] and $TiO_2(110)$[22] in ultrahigh vacuum (UHV), where the active sites have been identified as oxygen vacancies due to electron beam stimulated desorption (ESD) of oxygen; further examples are $Fe(CO)_5$ on thin porphyrin layers on Ag(111) in UHV,[23] and $Co_2(CO)_8$ on SiO_2 in HV.[24] It has also been shown that a self-assembled monolayer (SAM) can be activated by an electron beam for site

M. Drost, F. Tu, Prof. H. Marbach
Physikalische Chemie II
FAU Erlangen-Nürnberg
Egerlandstr. 3, 91058 Erlangen, Germany
E-mail: Hubertus.marbach@fau.de
Dr. F. Vollnhals
Advanced Instrumentation for Ion Nano-Analytics (AINA)
Luxembourg Institute of Science and Technology (LIST)
41 rue du Brill, L-4422 Belvaux, Luxembourg
I. Szenti, Prof. J. Kiss
MTA-SZTE Reaction Kinetics and Surface Chemistry Research Group
University of Szeged
Rerrich Béla sqr. 1, 6720 Szeged, Hungary

DOI: 10.1002/smtd.201700095

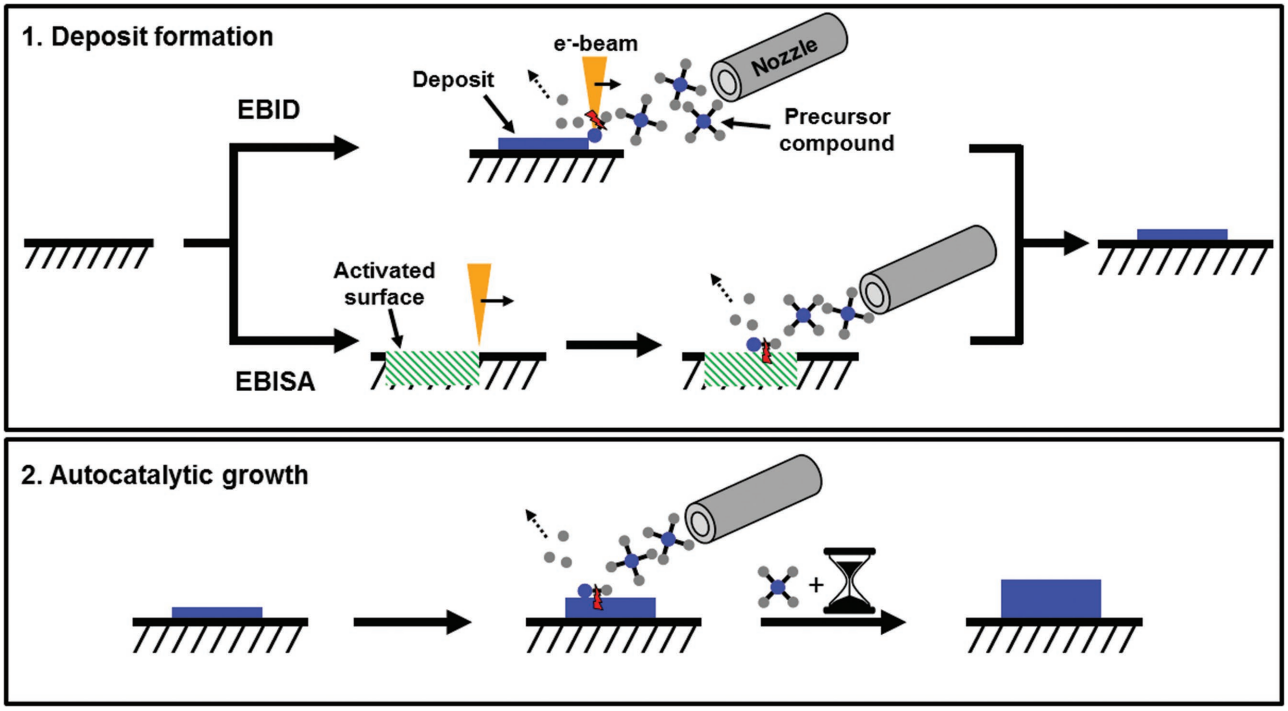

Figure 1. Idealized scheme of deposit formation using either EBID or EBISA and subsequent autocatalytic growth. 1) Deposit formation: in EBID, a precursor compound is dissociated by a focused e-beam and its interaction products with the bulk substrate, i.e., backscattered and secondary electrons crossing the substrate-vacuum interface. Dissociation products then either desorb from the surface or form a deposit at and close to the point of impact of the e-beam. In EBISA, the surface is irradiated by an e-beam in the absence of a precursor gas, resulting in chemically modified surface sites. A subsequently dosed precursor then decomposes selectively at pre-irradiated sites, leading to the formation of a deposit, whereas the nonirradiated surface remains unchanged. 2) Autocatalytic growth: the initially formed deposit is catalytically active, decomposing additionally supplied precursor molecules. The result is an effective increase in deposit size, while the catalytic activity is retained in the growth process.

selective material deposition using different techniques, e.g., electrodeposition[25] and atomic layer deposition (ALD).[26]

An essential requirement to control the deposit formation following EBISA is the ability of the initial deposit to grow autocatalytically, i.e., it has to be catalytically active toward the decomposition of an additionally supplied precursor, and retain the catalytic activity during the growth process, resulting in a deposit size increase (Figure 1(2)). In the case of $Fe(CO)_5$ at room temperature (RT), this leads the growth of cubic-shaped bcc-Fe crystals with an Fe content >95 at%.[21] Autocatalytic growth (AG), which can also occur on EBID structures, permits interesting processing strategies: in order to fabricate nanostructures on a larger scale, all structures can be grown in parallel after depositing a thin seed layer or activating the surface. This leads to a potentially higher throughput compared to the sole EBID process, where all material has to be deposited sequentially. Autocatalytic growth is essentially a chemical vapor deposition process, where the thermally induced precursor decomposition at a given processing temperature[27] is site selective. It has also been demonstrated that an ALD process, i.e., alternately dosing of $MeCpPtMe_3$ and O_2 at a substrate temperature of 300 °C, can be site selective on EBID deposits fabricated with the same precursor.[28,29] It is obviously a requirement for site selectivity that the rest of the substrate surface is inert toward the decomposition of the precursor. However, for a specific combination of precursor, substrate, and required processing parameters, unselective decomposition might occur. This is indeed the case for a variety of metal carbonyls, which are of particular interest in FEBIP due to anticipated favorable dissociation pathways, on certain substrates already at RT or below.[30–32]

In a recent study, we have shown that the catalytic activity of a Ag(111) surface toward the decomposition of $Fe(CO)_5$ can be inhibited by precovering the surface with a thin layer of 2H-tetraphenylporphyrin (2HTPP).[23] It is then possible to selectively fabricate clean Fe nanostructures using either EBID or EBISA procedures with $Fe(CO)_5$. We now expand this concept, showing that a thin 2HTPP layer prevents the unselective decomposition of $Co(CO)_3NO$ on rutile $TiO_2(110)$ 1×1 and Si(111) 7×7 at RT in UHV. Nanostructures from $Co(CO)_3NO$ can consequently be fabricated on the 2HTPP covered substrates with high site selectivity, using EBID and EBISA protocols and subsequent autocatalytic growth. We compare this procedure to FEBIP experiments on the same substrates with the precursor $Fe(CO)_5$, where the deposition is selective on both the pristine and the 2HTPP covered substrates. Additional FEBIP experiments performed on the reconstructed, pristine $TiO_2(110)$ 1×2 reveal that in contrast to the 1×1 surface, EBID with $Co(CO)_3NO$ is spatially selective, whereas $Fe(CO)_5$ dissociates and nucleates at 1×2 strands.[22] Scanning tunneling microscopy (STM) was employed for both, to image the $TiO_2(110)$ 1×2 surface and to ensure the formation of a closed layer of 2HTPP, and FEBIP deposits were characterized using scanning electron microscopy (SEM) and local Auger

electron spectroscopy (AES). Both precursors are chosen due to their property to grow autocatalytically,[21,33] their ease of handling, i.e., high vapor pressure, and especially due to the prospect to fabricate magnetic nanostructures.[15,34,35] Overall the present study reveals partially unexpected differences in the chemical selectivity of the two similar precursors and hints new protocols to fabricate nanostructures in a controlled manner.

2. Results and Discussion

FEBIP experiments were performed with $Co(CO)_3NO$ and $Fe(CO)_5$ on different substrates: Rutile $TiO_2(110)$ 1 × 1 and 1 × 2, Si(111) 7 × 7, and both $TiO_2(110)$ 1 × 1 and Si(111) 7 × 7 covered with a multilayer of 2HTPP with a thickness of 0.5–1.0 nm (2–3 layer). The autocatalytic growth time for all EBISA structures was 270 min, and is indicated in the corresponding captions. To guide the eye, a scheme of the corresponding system is depicted below each SEM image throughout the paper.

2.1. $TiO_2(110)$ 1 × 1 and 1 × 2

Summarized in **Figure 2** are SEM images of FEBIP deposits from $Co(CO)_3NO$ (panels (a–c)) and $Fe(CO)_5$ (panels (d–f)) on $TiO_2(110)$ 1 × 1. Figure 2a,b depicts square (4 × 4 μm^2) deposits, fabricated by EBISA and EBID, respectively, Figure 2c shows a nonirradiated surface site after an FEBIP experiment, i.e., after an exposure of ≈1.1 × 10^5 L of $Co(CO)_3NO$. It can be extracted that on the whole surface the formation of a thick film (i.e., substrate signals are completely attenuated in AES, cf. **Figure 3**) with granular morphology occurs without electron irradiation. A closely related AG experiment conducted on EBID deposits on an ultrathin Si_3N_4 membrane yielded a maximum thickness of 5 nm,[33] which would be probably sufficient to attenuate the AES signals from the bulk accordingly. In contrast to the previous investigation of $Fe(CO)_5$ on Ag(111), no preferred grain orientation induced by the underlying anisotropic surface can be observed. Based on AES measurements the composition of the deposit was estimated with ≈48 at% Co, ≈48 at% O, and minor amounts (<5 at%) of N and C (cf. Figure 3). Areas which were electron irradiated before (EBISA) or during (EBID) precursor dosage exhibit the same apparent morphology, however, they appear brighter in SEM (cf. Figure 2a,b). Local AES shows that the corresponding FEBIP areas contain a similar cobalt/oxygen ratio of ≈1:1, but no carbon, unlike the nonirradiated areas (Figure 3). To further investigate the peculiar role of the substrate an additional FEBIP experiment with $Co(CO)_3NO$ was performed on the reconstructed $TiO_2(110)$ 1 × 2. **Figure 4**a displays a scanning tunneling microscopy image of the surface prior to the experiment, and Figure 4b depicts the corresponding low-energy electron diffraction (LEED) pattern. The reconstructed surface basically consists of bright strands oriented in the [001]-direction.[36–38]

Figure 4c depicts the result of a 2 × 2 μm square EBID exposure with $Co(CO)_3NO$ and subsequent 60 min autocatalytic growth time (≈2.4 × 10^4 L $Co(CO)_3NO$). The actual

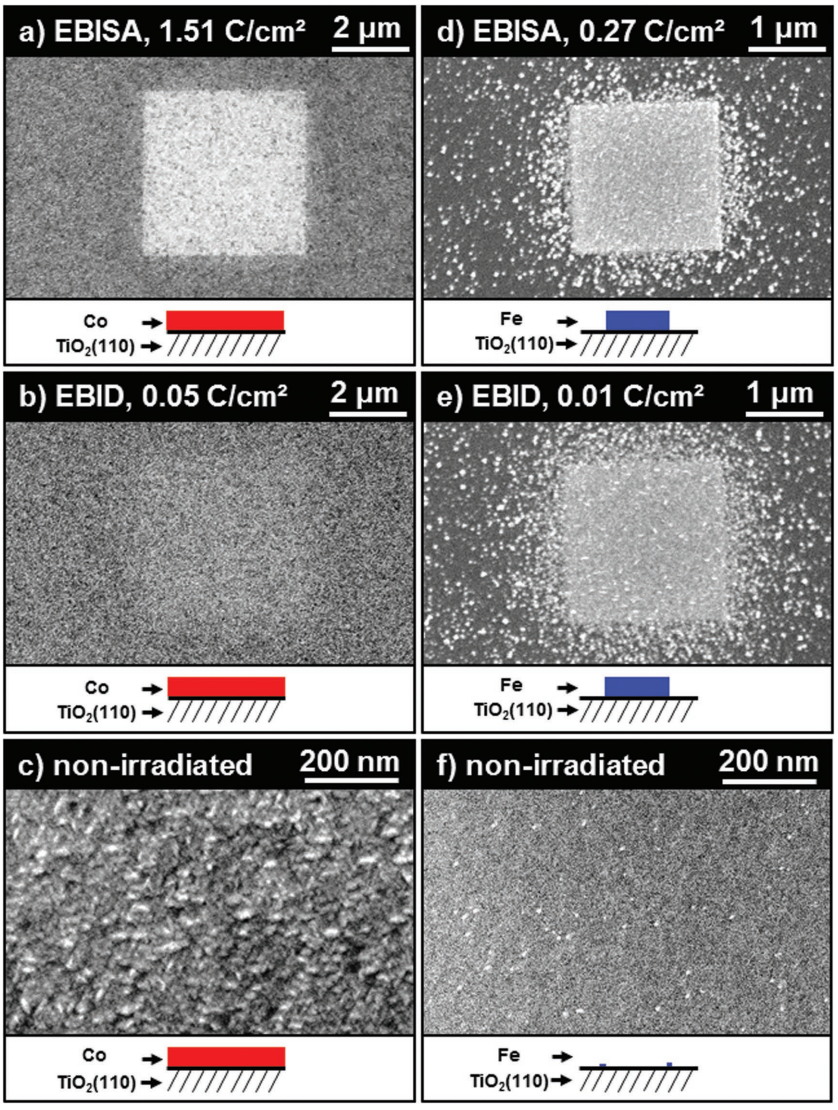

Figure 2. FEBIP on $TiO_2(110)$ 1 × 1. a) EBISA 4 × 4 μm^2 square from $Co(CO)_3NO$: a granular film has grown on the whole surface after a precursor exposure of ≈1.1 × 10^5 L: the pre-irradiated surface area appears brighter in SEM. b) EBID 4 × 4 μm^2 square from $Co(CO)_3NO$, autocatalytic growth time t_{AG} = 217 min: lower contrast and less defined boundaries compared to EBISA areas. c) Blowup of a nonirradiated surface area after the experiment with $Co(CO)_3NO$. d,e) EBISA and EBID (t_{AG} = 128 min) 2 × 2 μm^2 square deposits from $Fe(CO)_5$: deposition and autocatalytic growth of bcc-Fe is mainly confined to irradiated areas, unselective growth is only observed at surface defects. f) Blowup of a nonirradiated surface area after the experiment with $Fe(CO)_5$, again showing only sporadic unselective growth of bcc-Fe.

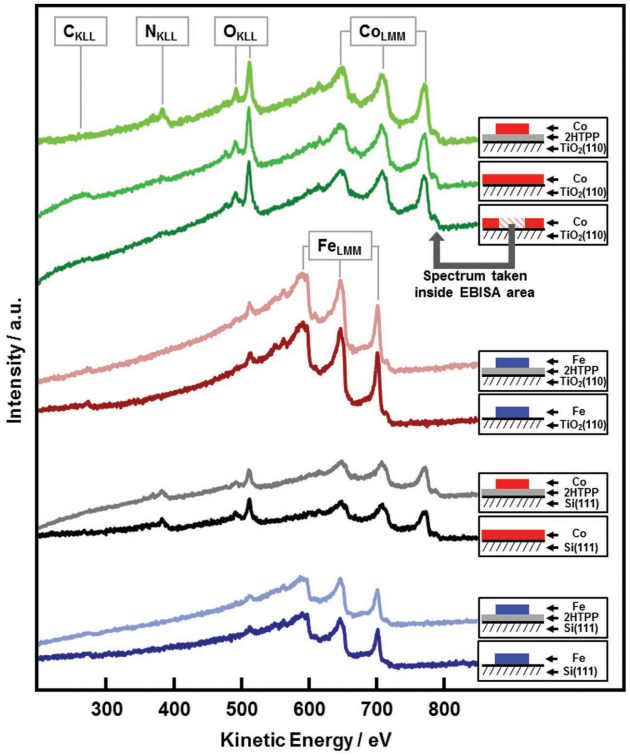

Figure 3. Local AE spectra from the different investigated systems, with the corresponding Auger transitions and schemes of the systems depicted. Spectra of the unselectively grown films from $Co(CO)_3NO$ were taken at random nonirradiated surface positions. For improved comparability by eye, all spectra were normalized (see the Experimental Section) to account for possible deviations originating from small differences in the measurement setup.

deposit extends beyond the irradiated area due to proximity effects and exhibits a pronounced SEM contrast. Local AES (Figure 4d, red) reveals that the deposit again consists of mostly Co and O as well as minor amounts of N and C, while AES recorded on a nonirradiated site (Figure 4d, blue) predominantly shows substrate signals and very minor Co. This finding clearly demonstrates that a more or less subtle surface modification can be sufficient to quench the catalytic activity of the latter.

The FEBIP experiments with $Fe(CO)_5$ on $TiO_2(110)$ 1×1 conducted in the work at hand are in agreement with our previous report,[22] and are presented and discussed in the context of the results obtained with $Co(CO)_3NO$ on the same substrate. Figure 2d,e depicts square (2×2 µm^2) deposits, fabricated by EBISA and EBID, Figure 2f shows again a nonirradiated area after an FEBIP experiment, i.e., after corresponding exposure to the precursor. The nonirradiated surface areas appear mostly uniform, with only few scattered cubic bcc-Fe crystallites (bright spots in the depicted images). The origins of this nonselective growth are local 1×2 reconstructed sites which act as nucleation centers, leading to the formation of pure bcc-Fe upon autocatalytic growth. However, the majority of the nonirradiated surface remains unchanged throughout the precursor exposure. The structures fabricated by FEBIP likewise consist of bcc-Fe crystallites formed by FEBIP and subsequent autocatalytic growth.[22] The Fe content of these deposits was estimated by AES as ≈95 at% with minor carbon and oxygen contaminations.

At low PE doses the crystallite formation is confined to electron beam irradiated areas, and exceeds them at higher PE doses due to proximity effects. As it has already been reported by Vollnhals et al. before,[23] deposit formation using EBISA requires higher PE doses compared to EBID in order to obtain similar sized deposits. This is presumably due to the absence of forward scattered electrons in EBISA, as well as the different deposit formation mechanisms, i.e., modification of the substrate in EBISA and direct precursor dissociation in EBID.

From these findings, we conclude the following: At RT, $TiO_2(110)$ 1×1 is catalytically active toward the decomposition of $Co(CO)_3NO$. The resulting overlayer formation is not self-limiting, i.e., catalytic activity is retained, leading to the formation of a thick granular film, remarkably consisting of approximately equal parts of cobalt and oxygen, as well as very minor amounts of carbon and nitrogen. The film deposition via AG appears to be sensitive to prior electron irradiation in particular via EBISA since it leads to less carbon being incorporated. This observation indicates that subtle differences in the starting material, e.g., induced by electron irradiation, influence the autocatalytic growth process, and the corresponding changes in composition are maintained in the deposition process and propagate through the material. The reason for the brighter appearance of the electron irradiated areas in Figure 2a,b remains unclear. Since the amount of carbon within the material grown on the nonirradiated areas is rather low (<5%) the so-called chemical contrast in SEM, which simply relates to brighter appearance with higher atomic number due to a higher backscattering coefficient of the latter is rather unlikely. Instead, we speculate that the presence of small amounts of carbon in the film might induce an increase of the local work function which would indeed yield the observed contrast. In this picture, the reduced amount of carbon in the Co containing deposit (as evidenced by AES shown in Figure 3) would directly explain the brighter appearance. In contrast to the findings with the Co precursor, FEBIP with $Fe(CO)_5$ on $TiO_2(110)$ 1×1 is highly selective. Deposit formation occurs almost exclusively at pre-irradiated surface sites (EBISA) following ESD of oxygen via the Knotek–Feibelman mechanism,[22,39] and at sites where EBID was performed. Interestingly, selective deposition in FEBIP can be also observed for $Co(CO)_3NO$ if the experiment is performed on a 1×2 reconstructed $TiO_2(110)$ surface. After an exposure ≈2.4×10^4 L $Co(CO)_3NO$, only traces of Co are detected on nonirradiated surface areas, probably due to remaining 1×1 surface areas which are not covered by 1×2 strands, as can be seen in the scanning tunneling microscopy image in Figure 4a. On the other hand, $Fe(CO)_5$ decomposes at 1×2 sites, and we anticipate the growth of a closed layer on a fully reconstructed 1×2 surface. The investigated systems therefore exhibit a prime example of how surface reconstructions can play an active role in the FEBIP process due to their catalytic activity, or lack of the latter, while this catalytic activity can severely differ even for chemically closely related precursors such as $Co(CO)_3NO$ and $Fe(CO)_5$.

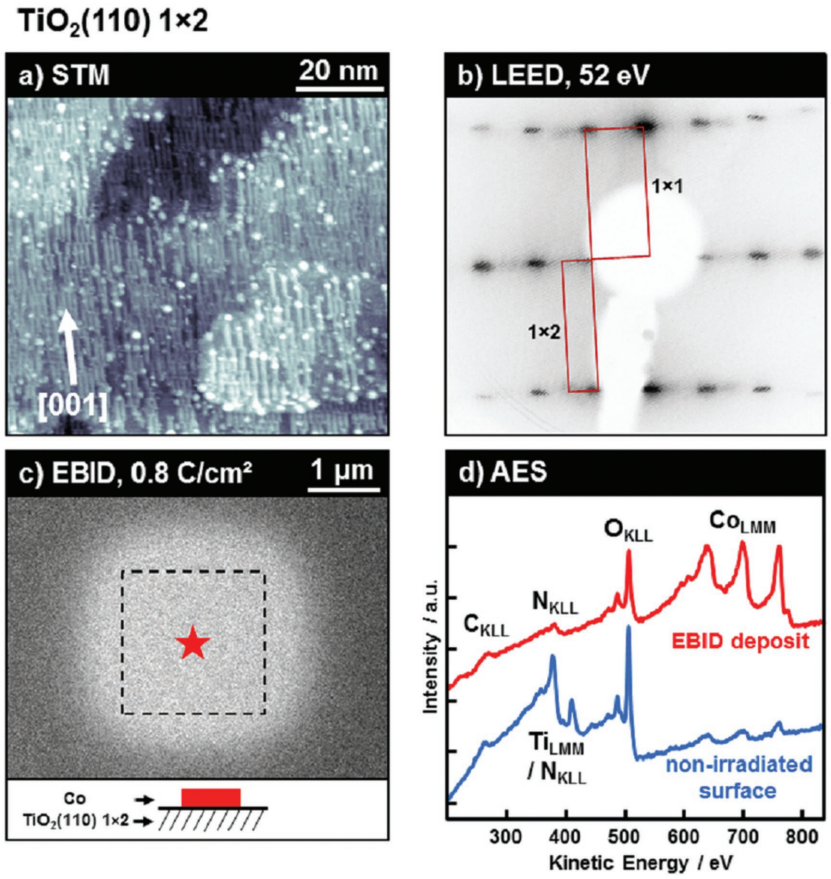

Figure 4. a) Scanning tunneling microscopy image of a TiO_2(110) 1 × 2 surface that was used as a substrate for an FEBIP experiment with $Co(CO)_3NO$. The reconstructed surface appears as bright strands which are oriented in the [001]-direction (U_{Bias} = 2.3 V, I = 1 nA). b) Corresponding LEED pattern, recorded at 52 eV. c) EBID 2 × 2 µm² square deposit from $Co(CO)_3NO$, t_{AG} = 60 min. Material deposition occurred outside the irradiated area (dashed frame) due to proximity effects. The red star indicates the position where local AES was conducted. d) AE spectra of the EBID deposit shown in (c) (red) and a nonirradiated surface site after the exposure to $Co(CO)_3NO$.

2.2. 2HTPP/TiO_2(110) 1 × 1

As demonstrated previously, a thin layer of organic molecules, namely 2HTPP, is suitable to act as a "protective capping," e.g., to prevent the unselective decomposition of $Fe(CO)_5$ on Ag(111) at RT. Consequently, this concept was transferred to the system $Co(CO)_3NO$ on TiO_2(110) 1 × 1, by covering the surface with a thin layer of 2HTPP (thickness 0.5–1.0 nm) prior to the FEBIP experiments. In a first step, STM was performed on a single layer of 2HTPP on the TiO_2. This was done to exclude a pronounced island (i.e., Volmer–Weber) growth, as the surface has to be fully covered for complete passivation (see Figure S1a and caption in the Supporting Information). **Figure 5**a–d depicts SEM images of FEBIP point deposits (i.e., the e-beam is kept stationary at one position for the indicated PE dose), using EBISA and EBID with both precursors, on TiO_2(110) covered with 2HTPP. Figure 5e shows the logo of the Excellence Cluster "Engineering of Advanced Materials," using EBID with $Co(CO)_3NO$, demonstrating the ability to lithographically fabricate structures with defined shape. It is obvious that FEBIP with $Co(CO)_3NO$ (Figure 5a,b,e) leads to deposit formation only at irradiated sites, whereas on the nonirradiated organic layer, no deposition is observed. All structures exhibit a granular morphology, and local AES (Figure 3) was used to estimate their composition to ≈50 at% Co, ≈40 at% O, and ≈10 at% N. The deposits grow autocatalytically, resulting in an increased thickness and slightly increased lateral extension upon prolonged precursor exposure.

Regarding the selectivity, FEBIP with $Fe(CO)_5$ shows the same results as observed before on the pristine surface, i.e., formation of crystalline bcc-Fe, again due to autocatalytic growth, is confined to sites where EBISA and EBID was performed, and the nonirradiated surface exhibits no changes. Local AES again shows an Fe content of ≈95 at% and only minor impurities of carbon and oxygen (Figure 3). Furthermore, we demonstrate that it is possible to fabricate line deposits with an average FWHM <32 nm (**Figure 6**a,b) using EBISA with $Co(CO)_3NO$ and <20 nm (Figure 6c,d) using EBID with $Fe(CO)_5$. The latter were fabricated using a relatively low autocatalytic growth time of 34 min to minimize structure broadening. This results in a deposit with granular morphology, clearly distinguishable from the crystalline morphology that follows prolonged autocatalytic growth. Note that the autocatalytic growth time for the EBISA line structures from $Co(CO)_3NO$ was 270 min, thus, the lateral extension of the corresponding deposits is not just simply a result of the autocatalytic growth time but is obviously more complex. For example, different growth rates for the different precursors as well as the chemical nature of the "seed" structure might contribute to the lateral extensions of the final deposit. However, we anticipate that the line widths can be further reduced by lowering the AG growth times. In addition, we want to emphasize that relatively little efforts were put into the reduction of the size of the corresponding FEBIP structures, which implies quite some room for improvements in this regard. The lithographic parameters are given in the Supporting Information.

From these results, we conclude that the organic layer effectively decouples the substrate from the FEBIP process. The catalytic activity, which in the case of $Co(CO)_3NO$ leads to the unselective decomposition and subsequent film growth at RT, is suppressed. The same applies for $Fe(CO)_5$ and its decomposition at 1 × 2 reconstructed sites. Instead, deposit formation is completely selective, and both EBID and EBISA protocols can be applied. We thus show for the first time that $Co(CO)_3NO$ is a suitable precursor for EBISA on thin porphyrin layers, i.e., the substrate can be activated by the electron beam. This is especially remarkable since EBISA did not work for $Co(CO)_3NO$ in previous experiments on SiO_x/Si(100) and

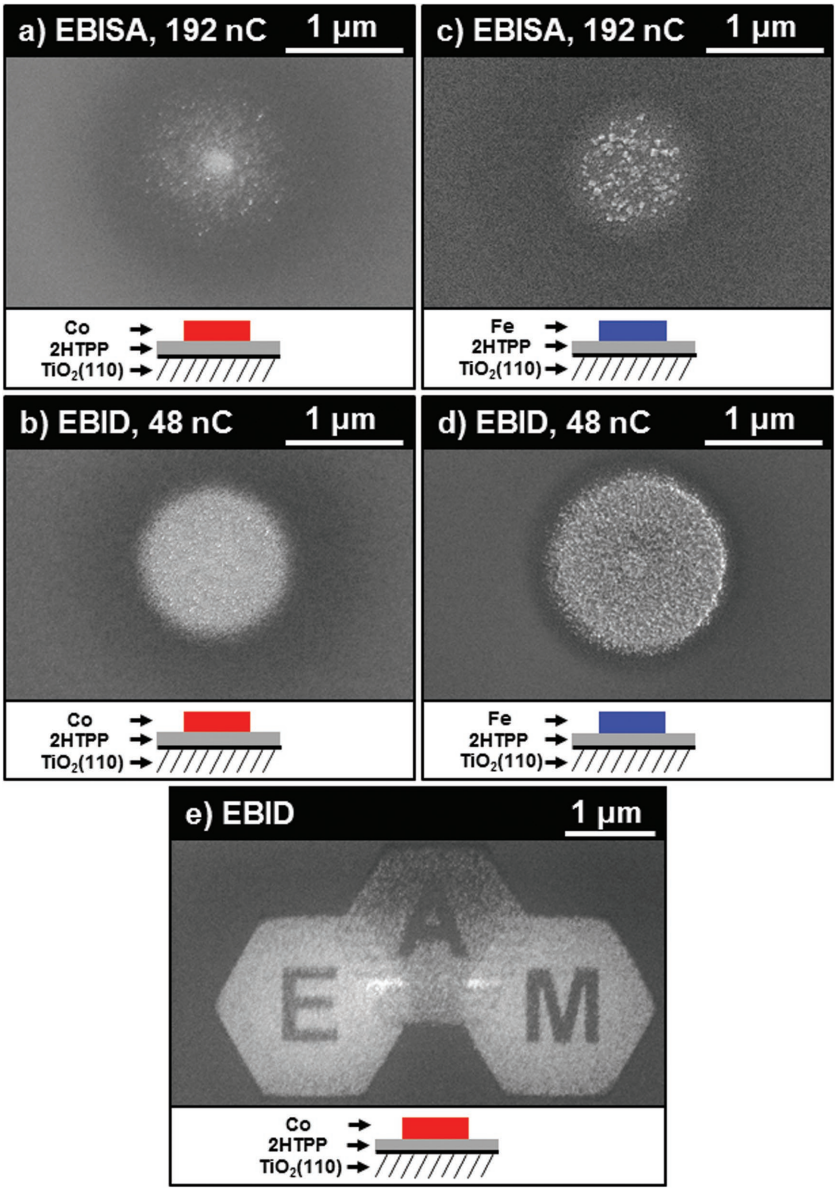

Figure 5. FEBIP on 2HTPP/TiO_2(110) 1 × 1. a,b) EBISA and EBID (t_{AG} = 215 min) point deposits, e) EBID area deposit (t_{AG} = 144 min) from $Co(CO)_3NO$ on 2HTPP/TiO_2(110). Nonirradiated surface areas exhibit a homogeneous SEM intensity, deposition and autocatalytic growth is confined to irradiated sites, and their surroundings due to proximity effects. c,d) EBISA and EBID (t_{AG} = 255 min) deposits from $Fe(CO)_5$: as with $Co(CO)_3NO$, deposition and autocatalytic growth of bcc-Fe is confined to irradiated sites.

SiO_x/Si_3N_4, substrates which worked well with $Fe(CO)_5$.[33] This aspect is interesting because it reflects a delicate chemical sensitivity of the EBISA process depending on the actual choice of one of the two precursors, which are otherwise apparently similar. Furthermore, the probed deposit sites fabricated from $Co(CO)_3NO$ contain no carbon, but a similar elemental composition compared to previous reports of FEBIP experiments with the same precursor,[33,40,41] i.e., about 50 at% Co and varying contents of O and N. We cannot conclude about the exact chemical nature of the deposits, however, a Co oxidation state higher than zero is likely, as it was reported for similar systems as well, e.g., for EBID and autocatalytic growth with $Co(CO)_3NO$ on Si_3N_4-membranes[33] and thermal decomposition of $Co_2(CO)_8$ on titanate nanowires.[42] The formation of carbon-free deposits from $Co(CO)_3NO$ on amorphous carbon was recently also reported in a UHV study by Rosenberg et al.[43] They observe the formation of $(CO)_xOCoN$ (x = 1–2) upon 500 eV electron irradiation of an adsorbed $Co(CO)_3NO$ layer at a substrate temperature of −168 °C. Upon annealing to RT, the remaining CO and carbon desorb, resulting in a carbon free CoO_yN species. Our data suggest the same elemental composition, thus, no carbon is incorporated during autocatalytic growth as well. When comparing the AE spectra of the systems Fe/2HTPP/TiO_2(110) and Fe/TiO_2(110) 1 × 1 (Figure 3), minor carbon impurities of similar intensity are observed. This suggests that in FEBIP deposits from both precursors, the carbon concentration is independent of the underlying 2HTPP layer. Despite the carbon-rich environment with the 2HTPP layer, no additional carbon is incorporated during the autocatalytic growth process, at least in the volume probed by AES.

At this point, we want to briefly discuss the possible electron beam activation mechanisms of the 2HTPP layer. To our knowledge, no detailed studies concerning the chemical modifications of thin porphyrin layers on surfaces upon electron beam irradiation have been conducted so far. With the available data, we cannot fully conclude on the chemical nature of the electron beam activation of the 2HTPP layer and the following precursor dissociation. However, some conclusions might be drawn from studies concerning electron beam irradiation of a variety of other organic compounds, mostly with a focus on low-energy electrons. Among others, the observed dissociation pathways include C—C chain scission and formation of diamond-like-carbon in undecylenic acid and 1-decene SAMs,[25] dehydrogenation and intermolecular cross-linking of aromatic groups in biphenyl thiol SAMs[44,45] and anion desorption from hydrocarbons following dissociative electron attachment.[46] Given the vast number of potential dissociation pathways, the effect of electron beam irradiation on a 2HTPP layer remains speculative. Possible reactions might be C—C bond scission and loss of the phenyl groups, dehydrogenation followed by C—C bond formations, accompanied by formation of reactive hydrocarbon species, such as radicals and ions.

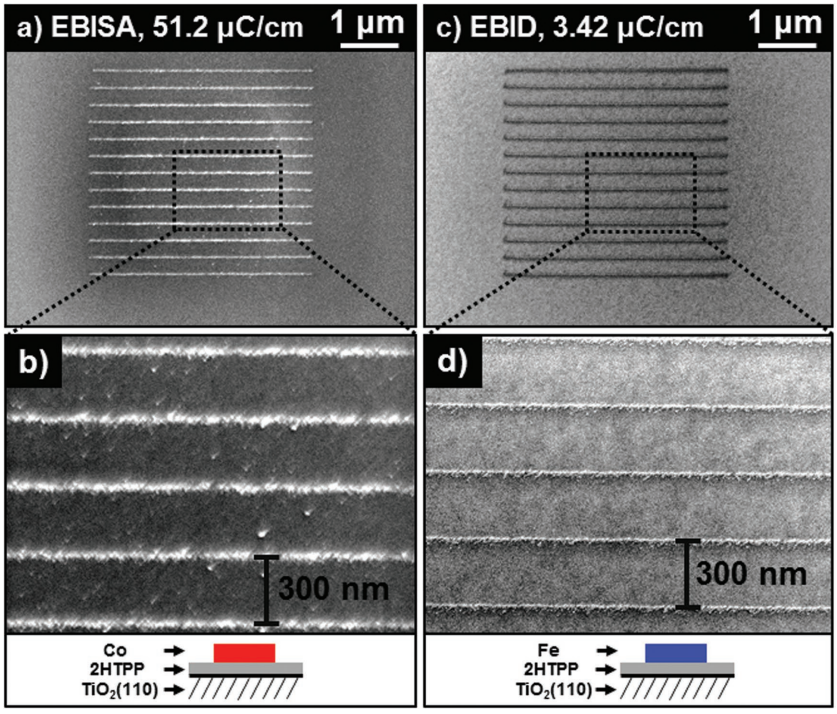

Figure 6. FEBIP on 2HTPP/TiO_2(110) 1 × 1. a,b) EBISA line structures (t_{AG} = 270 min) from $Co(CO)_3NO$ with an average FWHM <32 nm. Sporadically scattered deposits between the lines most likely result from proximity effects. c,d) EBID line structures (t_{AG} = 34 min) from $Fe(CO)_5$ with an average FWHM <20 nm; note the lack of crystalline bcc-Fe, due to the relatively low autocatalytic growth time compared to other FEBIP deposits shown in this work. For lithographic parameters, see Table S1 in the Supporting Information.

2.3. Si(111) 7 × 7 and 2HTPP/Si(111)

To expand the investigations to other substrates, FEBIP experiments with both precursors were performed on Si(111) 7 × 7 and 2HTPP/Si(111) 7 × 7. **Figure 7**a,b shows SEM images of EBID structures (4 × 4 µm^2 squares) fabricated from $Co(CO)_3NO$ and $Fe(CO)_5$, respectively, on Si(111) 7 × 7. Surprisingly, the deposition and autocatalytic growth of $Co(CO)_3NO$ is unselective similar to the observations on TiO_2(110) 1 × 1. That means the growth of a film with granular morphology can be observed on the entire surface. Chemical analysis of the latter by AES yields ≈51% cobalt, ≈34% oxygen, and ≈15% nitrogen, but no carbon, in contrast to the film grown on TiO_2(110) 1 × 1. Only a weak SEM contrast difference between areas where EBID was conducted and nonirradiated surface is observed, and both exhibit the same elemental composition (not shown).

In contrast, EBID with $Fe(CO)_5$ on Si(111) 7 × 7 is selective: deposition and growth of crystalline bcc-Fe (Fe content ≈95%) is only observed at irradiated sites, and partially their surroundings due to proximity effects. It has to be noted that with both precursors, EBISA is not possible on pristine Si(111) 7 × 7. For $Fe(CO)_5$ this is obviously again due to the lack of a suitable activation mechanism, i.e., e-beam irradiation does not lead to the formation of catalytically active surface sites. At the same time, $Co(CO)_3NO$ is immediately decomposed on Si(111) 7 × 7, which results in the observed unselective decomposition on the whole surface. Next, STM measurements ensured the formation of a closed layer of 2HTPP on Si(111) 7 × 7 (Figure S1b, Supporting Information). FEBIP experiments with both precursors were then performed on a 0.5–1.0 nm thick layer of 2HTPP on Si(111). The results are summarized in Figure 7b,c,e,f, which depict selected SE images, including the logo of the research unit FOR 1878 "funCOS" and a 4 × 4 µm^2 square deposit. In analogy to the system 2HTPP/TiO_2(110) 1 × 1, deposition is now confined to surface sites where FEBIP was conducted. Both EBISA and EBID protocols are successful, and autocatalytic growth is observed. Local AES shows deposits from $Co(CO)_3NO$ consist of ≈61% cobalt, ≈34% oxygen, and ≈12% nitrogen, while deposits from $Fe(CO)_5$ again consist of >95% iron and minor oxygen and carbon contributions.

We conclude that the delicate chemical sensitivity of the precursors and the concept of surface passivation with 2HTPP can be also transferred to the Si(111) 7 × 7 surface and appears to be of general character. Like on TiO_2(110) 1 × 1, the catalytic activity of the pristine surface toward the decomposition of $Co(CO)_3NO$ is suppressed by the thin organic layer, enabling the fabrication of nanostructures with high spatial selectivity. Unlike the pristine Si(111) 7 × 7, the 2HTPP layer is suitable for EBISA with $Co(CO)_3NO$ and $Fe(CO)_5$. This enables interesting nanofabrication strategies: all substrates that lack a suitable e-beam activation mechanism can be used for EBISA by covering it with a thin layer of 2HTPP, or another suitable compound. A requirement for this would be a sufficiently flat and clean pristine surface, such that the organic layer is completely closed and, ideally, grows in a layer-by-layer fashion. Due to the tendency to adsorb in a nearly flat lying fashion,[47] porphyrin derivatives generally appear to be good candidates for this approach. In this respect, we also anticipate that the passivation should work also for other molecular materials as long as they fully cover the surface and do not exhibit catalytic activity on their own.

3. Conclusion

Figure 8 illustrates the concept we have demonstrated in this work. At RT, the pristine surfaces of rutile TiO_2(110) 1 × 1 and Si(111) 7 × 7 are catalytically active toward the decomposition of the precursor $Co(CO)_3NO$, resulting in an unselective deposition and subsequent film growth at surface sites where no FEBIP was performed. Interestingly, we found that on TiO_2(110) 1 × 2, the situation significantly modified: no unselective deposition was observed with $Co(CO)_3NO$, except on remaining 1 × 1 areas. In contrast, FEBIP with $Fe(CO)_5$ on TiO_2(110) 1 × 1 and Si(111) 7 × 7 is spatially selective. This is especially remarkable, since one anticipates similar reactivities for the apparently similar precursors. However, it appears that the

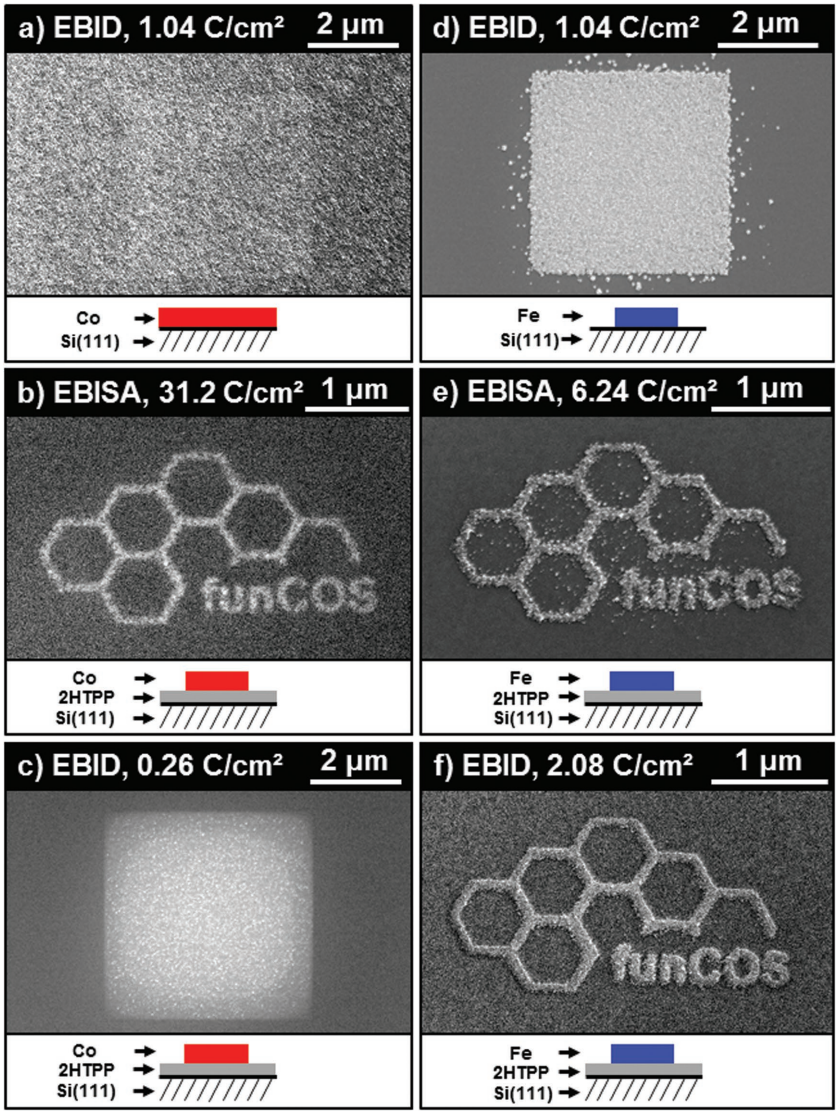

Figure 7. FEBIP on Si(111) 7 × 7 and 2HTPP/Si(111) 7 × 7. a) EBID 4 × 4 µm² square (t_{AG} = 246 min) from $Co(CO)_3NO$ on pristine Si(111) 7 × 7. Just as on TiO_2(110) 1 × 1, growth of a granular film is observed on the entire surface. Areas where FEBIP was performed exhibit the same morphology, with only a minor SEM brightness difference. b,c) EBISA and EBID (t_{AG} = 256 min) deposits from $Co(CO)_3NO$ on 2HTPP/Si(111) 7 × 7: deposition and autocatalytic growth is confined to irradiated areas. d) EBID 4 × 4 µm² square (t_{AG} = 252 min) from $Fe(CO)_5$ on pristine Si(111) 7 × 7. e,f) EBISA and EBID (t_{AG} = 256 min) deposits from $Fe(CO)_5$ on 2HTPP/Si(111) 7 × 7: on both substrates, deposition and autocatalytic growth of bcc-Fe is confined to irradiated areas.

sensitivity toward the corresponding surface sites is delicate. In that perspective, more efforts have to be made to understand the reactivity of such compounds on a fundamental level. One might envision to design precursor molecules for the selective decomposition at specific surface sites, which would open up new pathways for the controlled fabrication of well-defined nanostructures. The decomposition of $Co(CO)_3NO$ can be prevented by precovering the surface with a thin layer (0.5–1.0 nm) of 2HTPP. This organic layer is a suitable substrate for highly site selective deposition and autocatalytic growth with both precursors, using either of the EBID or EBISA procedures. Local AES of these deposits indicates that despite the carbon-rich environment, no carbon incorporation during autocatalytic growth occurs. Line structures on 2HTPP/TiO_2(110) with an average FWHM <32 nm (EBISA with $Co(CO)_3NO$) and <20 nm (EBID with $Fe(CO)_5$) were fabricated, showing that it is possible to fabricate nanoscale structures in a controlled manner on this surface. These results expand the applicability of EBISA, by showing for the first time that $Co(CO)_3NO$ is a suitable precursor for the method, in addition to the precursors $Fe(CO)_5$ and $Co_2(CO)_8$ that have already been shown to work.[19,24] Even a substrate that lacks a suitable e-beam activation mechanism, i.e., Si(111) 7 × 7, can be used for EBISA by precovering it, e.g., with 2HTPP and activating the thin organic layer. Even though the detailed chemical mechanisms are not yet fully understood, it is clear that the present findings significantly expand the scope of FEBIP and open several novel pathways for controlled nanofabrication. For example, one might envision using the thin organic layer in only one processing step, i.e., for passivation or "enabling" EBISA, and then thermally desorb it after the FEBIP step. A requirement for this would be sufficiently low desorption temperature in order to prevent thermal decomposition of the FEBIP deposits. Another idea is to use molecular architectures, e.g., from porphyrins, which form supramolecular well-ordered structures with, e.g., regular pores in the single digit nanometer-regime.[48,49] At the pores the surface is consequently exposed and thus potentially active toward the corresponding decomposition of precursor molecules. In this way, regular pattern of catalytically deposited material might be realized with dimensions well below the usual structures fabricated with FEBIP protocols. Furthermore, the presented results indicate that EBISA is applicable on every substrate by preparation of a thin porphyrin layer.

4. Experimental Section

All experiments were performed in a commercial UHV system (Multiscanlab, Omicron Nanotechnology, Germany) with a base pressure of $p < 2 \times 10^{-10}$ mbar. The main component of the analysis chamber is a UHV-compatible electron column (Leo Gemini) for SEM with a nominal resolution better than 3 nm and, in combination with a hemispherical electron energy analyzer, local AES and scanning Auger microscopy with a resolution better than 10 nm. In addition, an STM scanner and tip can be inserted between the pole piece of the SEM column and the sample to allow in situ STM measurements and tip positioning using the SEM. STM tips were prepared by cutting a 0.25 mm Pt/Ir wire, and used without further treatment. $Fe(CO)_5$

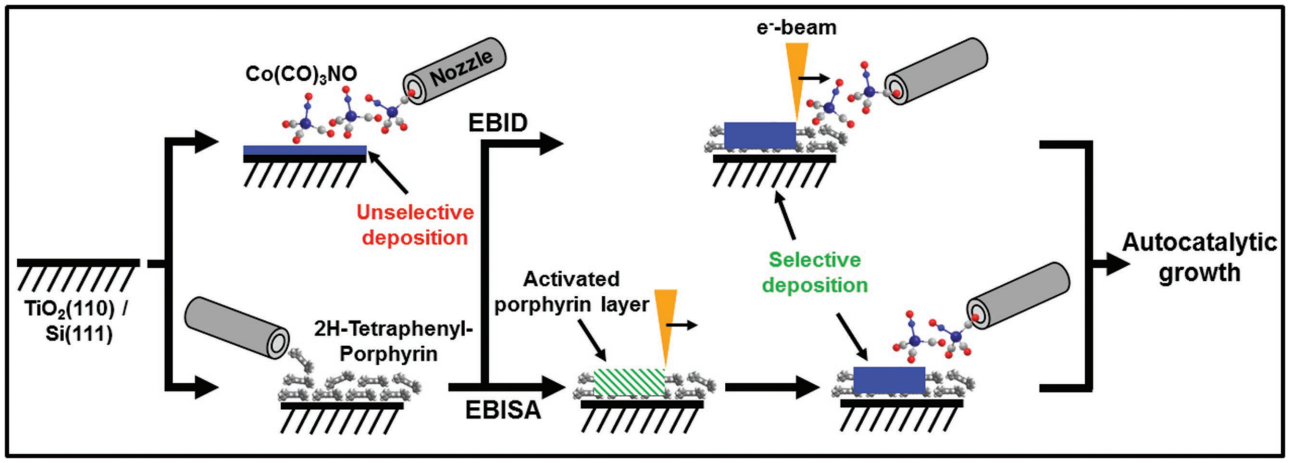

Figure 8. Scheme of the concept of surface passivation. Upon dosing of $Co(CO)_3NO$ on either rutile $TiO_2(110)$ 1×1 or Si(111) 7×7, unselective precursor decomposition and film growth takes place. By covering the pristine surface with a thin layer of 2HTPP, the catalytic activity of the surface is suppressed. Instead, nanostructures can be fabricated with high site selectivity, using either of the EBID or EBISA routines and subsequent autocatalytic growth. The depicted procedure of FEBIP on 2HTPP covered substrates also works with $Fe(CO)_5$.

was purchased from ACROS Organics, $Co(CO)_3NO$ from abcr GmbH & Co. KG. The quality of the precursor gas was analyzed with a quadrupole mass spectrometer in a dedicated gas analysis chamber (base pressure $<2 \times 10^{-9}$ mbar). The precursor gas was dosed through a nozzle with an inner diameter of 3 mm, and a distance of ≈12 mm to the sample surface. Based on simulations with the software GIS Simulator (version 1.5),[50] the local pressure increase on the sample surface of about 30× was estimated. For a fixed background pressure of 3.0×10^{-7} mbar, this corresponds to a local pressure at the surface of about 9×10^{-6} mbar. Rutile $TiO_2(110)$ crystals were purchased from CrysTec (Berlin, Germany), and prepared by repeated cycles of Ar ion sputtering (1 keV, 4×10^{-6} mbar) and annealing to 1040 and 1080 K to obtain the 1×1 and 1×2 surfaces, respectively. Laser-cut Si(111) wafers were purchased from the Institute of Electronic Materials Technology (Warsaw, Poland). They were cleaned by repeated flashing of the sample in UHV up to ≈1500 K. The surface quality of the samples used was assessed by LEED and STM, while the surface composition was checked with wide scan AES. 2H-Tetraphenylporphyrin powder was purchased from Porphyrin Systems (purity 98%) and deposited onto the freshly prepared substrates via a self-constructed Knudsen cell evaporator at an evaporation temperature of ≈580 K. Quantitative values about the deposit compositions given in the text were deduced from the relevant peak areas after background subtraction divided by the corresponding element- and transition-specific sensitivity factors. The estimation of layer thicknesses was performed using the modified straight-line approximation model, as described in Equations (2) and (15) in the work of Cumpson and Seah.[51] Electron exposures for SEM and lithography were done at a beam energy of 15 keV and nominal probe currents of 400 pA (EBID) and 3 nA (EBISA). The lithographic processes were controlled via a self-made lithography application based on LabView 8.6 (National Instruments) and a high-speed DAC PCIe-card (M2i.6021-exp, Spectrum GmbH, Germany). All given electron doses were corrected to account for probe current deviations which were measured using a Faraday cup. SEM images were acquired with SmartSEM (Zeiss) and are shown with minor contrast and brightness adjustments only. For Auger electron spectroscopy, the electron beam of the SEM was used as ionization source, with a beam energy of 15 keV and a nominal probe current of 3 nA. Spectra were recorded with a hemispherical electron energy analyzer (EA125, Omicron Nanotechnology) and Matrix 3.1 (Omicron Nanotechnology). Data processing was performed with Igor Pro 6.22A (Wavemetrics). The depicted spectra were normalized such that all spectra from the same substrate have the same intensity at E_{Kin} = 805 eV. ST images were acquired using Matrix 3.1.1 (Omicron Nanotechnology) and evaluated using the latest versions of WSxM.[52]

Supporting Information

Supporting Information is available from the Wiley Online Library or from the author.

Acknowledgements

The authors thank Prof. Hans-Peter Steinrück from the Chair of Physical Chemistry II (Friedrich-Alexander-Universität Erlangen-Nürnberg) and Prof. Zoltán Kónya from the Department of Applied and Environmental Chemistry (University of Szeged) for fruitful discussions. This work was supported by the research unit FOR1878/funCOS, the DFG through Grant No. MA 4246/1-2, project D7 of the Excellence Cluster "Engineering of Advanced Materials" granted to the FAU Erlangen-Nürnberg, COST Action CM1301 (CELINA), OTKA K120115, GINOP-2.3.2-15-2016-00013, and the Alexander von Humboldt Foundation within the Research Group Linkage Programme.

Conflict of Interest

The authors declare no conflict of interest.

Keywords

cobalt tricarbonyl nitrosyl, electron beam induced deposition, electron-beam-induced surface activation, iron pentacarbonyl, nanofabrication

Received: February 6, 2017
Revised: March 31, 2017
Published online:

[1] W. F. van Dorp, C. W. Hagen, *J. Appl. Phys.* **2008**, *104* , 081301.
[2] S. J. Randolph, J. D. Fowlkes, P. D. Rack, *Crit. Rev. Solid State Mater. Sci.* **2006**, *31*, 55.

[3] I. Utke, P. Hoffmann, J. Melngailis, *J. Vac. Sci. Technol., B* **2008**, *26*, 1197.
[4] K. Murakami, F. Wakaya, M. Takai, *J. Vac. Sci. Technol., B* **2007**, *25*, 1310.
[5] I. Utke, P. Hoffmann, R. Berger, L. Scandella, *Appl. Phys. Lett.* **2002**, *80*, 4792.
[6] K. Edinger, H. Becht, J. Bihr, V. Boegli, M. Budach, T. Hofmann, H. W. P. Koops, P. Kuschnerus, J. Oster, P. Spies, B. Weyrauch, *J. Vac. Sci. Technol., B* **2004**, *22*, 2902.
[7] T. H. P. Chang, *J. Vac. Sci. Technol.* **1975**, *12*, 1271.
[8] D. J. Burbridge, S. N. Gordeev, *Nanotechnology* **2009**, *20*, 285308.
[9] H. Plank, D. A. Smith, T. Haber, P. D. Rack, F. Hofer, *ACS Nano* **2012**, *6*, 286.
[10] W. F. Van Dorp, S. Lazar, C. W. Hagen, P. Kruit, *J. Vac. Sci. Technol., B* **2007**, *25*, 1603.
[11] K. Mitsuishi, M. Shimojo, M. Takeguchi, M. Tanaka, K. Furuya, *Jpn. J. Appl. Phys.* **2006**, *45*, 5517.
[12] M.-M. Walz, F. Vollnhals, F. Rietzler, M. Schirmer, H.-P. Steinrück, H. Marbach, *Appl. Phys. Lett.* **2012**, *100*, 053118.
[13] M. Weber, H. W. P. Koops, M. Rudolph, J. Kretz, G. Schmidt, *J. Vac. Sci. Technol., B* **1995**, *13*, 1364.
[14] T. Lukasczyk, M. Schirmer, H.-P. Steinrück, H. Marbach, *Small* **2008**, *4*, 841.
[15] A. Fernández-Pacheco, J. M. De Teresa, R. Córdoba, M. R. Ibarra, *J. Phys. D: Appl. Phys.* **2009**, *42*, 055005.
[16] M. M. Shawrav, P. Taus, H. D. Wanzenboeck, M. Schinnerl, M. Stöger-Pollach, S. Schwarz, A. Steiger-Thirsfeld, E. Bertagnolli, *Sci. Rep.* **2016**, *6*, 1.
[17] A. Botman, J. J. L. Mulders, C. W. Hagen, *Nanotechnology* **2009**, *20*, 1.
[18] H. Marbach, *Appl. Phys. A* **2014**, *117*, 987.
[19] a) M.-M. Walz, M. Schirmer, F. Vollnhals, T. Lukasczyk, H.-P. Steinrück, H. Marbach, *Angew. Chem.* **2010**, *122*, 4774; b) *Angew. Chem., Int. Ed.* **2010**, *49*, 4669.
[20] M.-M. Walz, F. Vollnhals, F. Rietzler, M. Schirmer, A. Kunzmann, H.-P. Steinrück, H. Marbach, *J. Phys. D: Appl. Phys.* **2012**, *45*, 1.
[21] M.-M. Walz, F. Vollnhals, M. Schirmer, H.-P. Steinrück, H. Marbach, *Phys. Chem. Chem. Phys.* **2011**, *13*, 17333.
[22] F. Vollnhals, T. Woolcot, M.-M. Walz, S. Seiler, H.-P. Steinrück, G. Thornton, H. Marbach, *J. Phys. Chem. C* **2013**, *117*, 17674.
[23] F. Vollnhals, P. Wintrich, M.-M. Walz, H.-P. Steinrück, H. Marbach, *Langmuir* **2013**, *29*, 12290.
[24] K. Muthukumar, H. O. Jeschke, R. Valenti, E. Begun, J. Schwenk, F. Porrati, M. Huth, *Beilstein J. Nanotechnol.* **2012**, *3*, 546.
[25] E. Balaur, T. Djenizian, R. Boukherroub, J. N. Chazalviel, F. Ozanam, P. Schmuki, *Electrochem. Commun.* **2003**, *6*, 153.
[26] J. Huang, M. Lee, J. Kim, *J. Vac. Sci. Technol., A* **2012**, *30*, 01A1281.
[27] E. E. Finney, R. G. Finke, *J. Colloid Interface Sci.* **2007**, *317*, 351.
[28] A. J. M. Mackus, J. J. L. Mulders, M. C. M. van de Sanden, W. M. M. Kessels, *J. Appl. Phys.* **2010**, *107*, 116102.
[29] A. J. M. Mackus, S. A. F. Dielissen, J. J. L. Mulders, W. M. M. Kessels, *Nanoscale* **2012**, *4*, 4477.
[30] F. Zaera, *Surf. Sci.* **1990**, *255*, 280.
[31] M. Xu, F. Zaera, *J. Vac. Sci. Technol., A* **1996**, *14*, 415.
[32] T. Lukasczyk, M. Schirmer, H.-P. Steinrück, H. Marbach, *Langmuir* **2009**, *25*, 11930.
[33] F. Vollnhals, M. Drost, F. Tu, E. Carrasco, A. Späth, R. Fink, H.-P. Steinrück, H. Marbach, *Beilstein J. Nanotechnol.* **2014**, *5*, 1175.
[34] J. M. De Teresa, A. Fernández-Pacheco, R. Córdoba, L. Serrano-Ramón, S. Sangiao, M. R. Ibarra, *J. Phys. D: Appl. Phys.* **2016**, *49*, 243003.
[35] F. Tu, M. Drost, F. Vollnhals, A. Späth, E. Carrasco, R. H. Fink, H. Marbach, *Nanotechnology* **2016**, *27*, 355302.
[36] R. A. Bennett, P. Stone, N. J. Price, M. Bowker, *Phys. Rev. Lett.* **1999**, *82*, 3831.
[37] S. Takakusagi, K. Fukui, F. Nariyuki, Y. Iwasawa, *Surf. Sci.* **2003**, *523*, L41.
[38] U. Diebold, *Surf. Sci. Rep.* **2002**, *48*, 53.
[39] M. L. Knotek, P. J. Feibelman, *Phys. Rev. Lett.* **1978**, *40*, 964.
[40] G. C. Gazzadi, H. Mulders, P. Trompenaars, A. Ghirri, M. Affronte, V. Grillo, S. Frabboni, *J. Phys. Chem. C* **2011**, *115*, 19606.
[41] G. C. Gazzadi, J. J. L. Mulders, P. Trompenaars, A. Ghirri, A. Rota, M. Affronte, S. Frabboni, *Microelectron. Eng.* **2011**, *88*, 1955.
[42] D. Madarász, G. Pótári, A. Sápi, B. László, C. Csudai, A. Oszkó, À. Kukovecz, A. Erdőhelyi, Z. Kónya, J. Kiss, *Phys. Chem. Chem. Phys.* **2013**, *15*, 15917.
[43] S. G. Rosenberg, M. Barclay, D. H. Fairbrother, *J. Phys. Chem. C* **2013**, *117*, 16053.
[44] A. Turchanin, D. Käfer, M. El-Desawy, C. Wöll, G. Witte, A. Gölzhäuser, *Langmuir* **2009**, *25*, 7342.
[45] W. Geyer, V. Stadler, W. Eck, M. Zharnikov, A. Gölzhäuser, M. Grunze, *Appl. Phys. Lett.* **1999**, *75*, 2401.
[46] L. Sanche, *Nucl. Instrum. Methods Phys. Res., Sect. B* **2003**, *208*, 4.
[47] J. V. Barth, G. Costantini, K. Kern, *Nature* **2005**, *437*, 671.
[48] a) J. A. A. W. Elemans, S. Lei, S. De Feyter, *Angew. Chem.* **2009**, *121*, 7434; b) *Angew. Chem., Int. Ed.* **2009**, *48*, 7298.
[49] D. Bonifazi, A. Kiebele, M. Stöhr, F. Cheng, T. Jung, F. Diederich, H. Spillmann, *Adv. Funct. Mater.* **2007**, *17*, 1051.
[50] V. Friedli, I. Utke, *J. Phys. D: Appl. Phys.* **2009**, *42*, 1.
[51] P. J. Cumpson, M. P. Seah, *Surf. Interface Anal.* **1997**, *25*, 430.
[52] I. Horcas, R. Fernández, J. M. Gómez-Rodríguez, J. Colchero, J. Gómez-Herrero, A. M. Baro, *Rev. Sci. Instrum.* **2007**, *78*, 0137051.

